applied sciences

MDPI

Article

A Collection of Formulae for the Design of Compton Back-Scattering X-ray Sources

Giuseppe Dattoli [1], Emanuele Di Palma [1,*] and Vittoria Petrillo [2,3,4]

[1] Department of Nuclear Fusion, ENEA Frascati Research Center, Via Enrico Fermi 45, 00044 Rome, Italy
[2] INFN Milano, Via Celoria 16, 20133 Milano, Italy
[3] LASA, Via F. Cervi 201, Segrate, 20090 Milano, Italy
[4] Department of Physics, Università degli Studi di Milano, Via Celoria 16, 20133 Milano, Italy
* Correspondence: emanuele.dipalma@enea.it; Tel.: +39-06-9400-5709

Abstract: Along with the development of FEL X-ray sources, the design and the construction of Compton Back-Scattering (CBS) devices for different applications are being pursued. These sources are designed to provide monochromatic, high peak brightness tunable light beams, with photon energies above 10 *KeV*. The source brightness is the most significant figure of merit, which specifies the suitability of X-ray beams for their application in a specific field of interest and also reflects the quality of the electron beam itself, which in turn depends on the charge, emittance, energy spread, etcetera. This article is intended as an introductory review to the field and we embed a few theoretical considerations and analytical formulae to develop simple tools for the design of CBS X-ray sources. The present attempt is analogous to previous efforts, put forward to model Free Electron Laser devices, using scaling relations accounting for the entanglement between the different physical quantities contributing to the output beam performances. We comment on the reliability of our analysis by a comparison with the wealth of results (either numerical and analytical) reported in the dedicated literature.

Keywords: RF wave undulator; free electron laser; Thomson back scattering; linac; X-ray; Compton back scattering

Citation: Dattoli, G.; Di Palma, E.; Petrillo, V. A Collection of Formulae for the Design of Compton Back-Scattering X-ray Sources. *Appl. Sci.* **2023**, *13*, 2645. https://doi.org/10.3390/app13042645

Academic Editor: Cristian De Santis

Received: 5 January 2023
Revised: 14 February 2023
Accepted: 16 February 2023
Published: 18 February 2023

1. Introduction

Free Electron Laser (FEL) [1] and Compton Back Scattering (CBS) [2] devices are complex systems, which embed different physical environments, characterized by a large number of specific parameters. The relevant theoretical description, necessarily non trivial, requires massive numerical simulations to explore the associated phenomenology and the design details. The use of scaling formulae [3–6] has played an important role in the design of FEL devices operating in the SASE and oscillator configurations and has been recently employed to discuss the feasibility of FELs driven by plasma-accelerated beams.

The logical steps underlying the reported strategy are summarized in Figure 1. Namely, scaling/empirical formulae are used to determine the space of parameters fixing the working point, and home-made/commercially available codes are used to refine the first evaluation and eventually to benchmark the first step.

CBS X-ray devices aim at providing sources of photons with energy above tens of *keV* with adequate luminosity. In this review, we collect different ideas, provided in the past, by several Authors, regarding Compact Light Sources and present the basic tools for fixing the working point of an actual CBS-based device.

The elementary physical mechanism underlying devices of this type is the head-on collision of a (sufficiently) energetic beam with a (sufficiently) intense and coherent optical source [7]. The latter may also be provided by the field of an undulator, which is seen by the electrons as a coherent ensemble of photons [8,9].

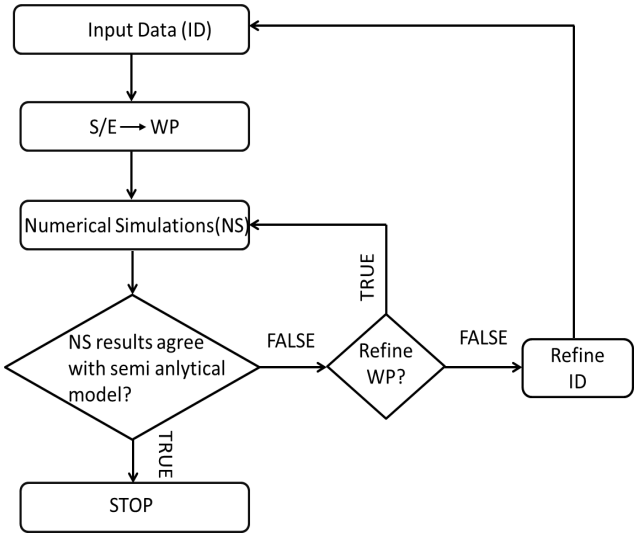

Figure 1. FEL design strategy flow chart: (1) Input data (beam and undulator parameters and the desired wavelength emission) (2) $S/E \longrightarrow WP$ = use of Scaling/Empirical formula to find the working point (3) Numerical Simulations (NS) = use of numerical codes to refine the details of the preliminary definition of the space parameters (4) Loop the process, changing the input data and/or the working point, until the benchmark with semi-analytical model is true.

The geometry of the CBS process is reported in Figure 2. The energy of the backscattered photon ($\mathcal{E}_s$) in terms of the laser/electron energies($\mathcal{E}_l, E_e$), of the electron kinematic variables ($\beta,\ \gamma$) and of the scattering angles ($\vartheta_{i,f}$ see Figure 2) is specified by (the polarization of the scattered photons is essentially that of the input field)

$$\mathcal{E}_s = \frac{(1-\beta\ \cos(\vartheta_i))\mathcal{E}_l}{(1-\beta\cos(\vartheta_f)) + \dfrac{\mathcal{E}_l}{E_e}(1-\cos(\vartheta_f-\vartheta_i))}. \tag{1}$$

For the details of the symbols, notations and abbreviations see Nomenclature, if not explicitly mentioned in the text.

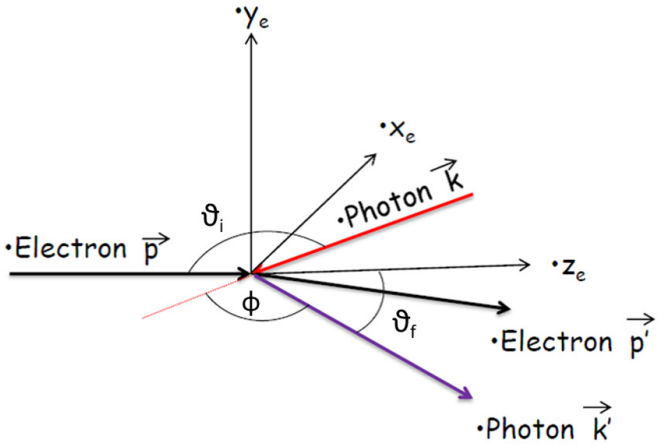

Figure 2. Kinematic and geometric variables of Compton Backscattering: input ($\vec{p}$) and output ($\vec{p}'$) electron momenta, $\vec{k}, \vec{k}'$ wave vectors of incident and scattered photon, respectively; orientation and amplitude of the incident θ_i, scattered θ_f photon angles and $\phi = \theta_i - \theta_f$ relative difference.

The wavelength of the scattered radiation for a head-on diffusion ($\vartheta_i \cong \pi$, $\vartheta_f \cong 0$), for (ultra-)relativistic electrons ($\beta \cong 1 - \frac{1}{2\gamma^2}$) and in the Thomson limit (assuming $E_e \ll \mathcal{E}_l$) is

$$\lambda_s = \frac{\lambda_l}{4\gamma^2}. \tag{2}$$

For further comments on the scattering geometry and the relevant kinematics, we address the reader to ref. [10].

It should be mentioned that, albeit we refer to the process under study as "Compton" scattering, most of our forthcoming discussion applies to the Thomson scattering, namely the physical conditions in which the quantum recoil and hence the ratio $\mathcal{E}_l/E_e$ does not play any role. We find indeed that the "quantum" term correction $\mathcal{E}_l/E_e = \lambda\!\!\!^{-}_c/(\gamma\lambda_l) << 1$ is negligible for the experimental conditions discussed here.

The mechanism, underlying the emission of bremsstrahlung photons by relativistic electrons moving inside a magnetic undulator, can be traced back to the same microscopic process (see Figure 3).

Figure 3. Emissionin undulator macroscopic picture (**left**) and microscopic picture (**right**); IP stands for interaction point.

The undulator is a device characterized by an alternating magnetic field, with a spatial period λ_u. The use of the Fermi-Weiszacker-Williams [11–13] approximation was the starting point of the Madey seminal paper [1], which signed the modern point of view to the FEL. In more practical terms, the process of photon emission in the undulator can be considered as the head-on collision of a "pseudo" photon with wavelength

$$\lambda^* = 2\lambda_u, \tag{3}$$

and an electron with the relativistic factor defined as

$$\gamma^* = \frac{\gamma}{\sqrt{1 + \frac{K_u^2}{2}}}. \tag{4}$$

According to Equation (2), we find for the wavelength of the radiated photons

$$\lambda_s = \frac{\lambda_u}{2\gamma^2}\left(1 + \frac{K_u^2}{2}\right). \tag{5}$$

From the point of view of the elementary mechanisms, the role of the undulator-strength parameter is that of including, in the scattering process, the contribution of the scattered wave photon density [14–25]. It is evident that an analogous term (sometimes called Kibble shift) should also appear in Equation (2). The laser field strength parameter is of noticeable importance for our discussion and, in terms of the laser intensity, reads (we use K_l instead of a_0 to denote the laser strength parameter either for continuity reasons with the notation of our previous papers or to underline the quasi complete equivalence with the undulator parameter)

$$K_l = \frac{eE_l\lambda_l}{2\pi m_e c^2}, \tag{6}$$

where E_l is the peak electric field associated with the laser. In practical units, the Equation (6) is usually written as

$$K_l \cong 8.5 \times 10^{-15} \lambda_l[nm] \sqrt{I_l \left[\frac{W}{m^2}\right]}, \tag{7}$$

with λ_l and I_l being the laser wavelength (expressed in nanometer) and the intensity expressed in W/m^2, respectively.

The laser strength parameter K_l is a key quantity determining the regime of operation of the scattering process itself (for further comments see the second part of the paper). In order to give an idea of the involved orders of magnitude, we note that for an Infrared Laser, ($\lambda \approx 1$ μm) $K_l = 0.1$ corresponds to a laser intensity slightly larger than 10^{18} W/m^2.

Even though the process shown in Figure 2 reports a single photon-single electron scattering, in a CBS device, the interaction occurs between the N_e (non interacting) electrons composing the electron bunch and the N_l photons contributing to the laser field. The flux of the scattered X-ray photons ($\dot{N}_x$) in a head-on scattering depends on the total cross section of the process and on the luminosity (L_0), a pivotal quantity including the numbers of electrons and photons, namely

$$\dot{N}_x \cong \sigma_{Th} \cdot L_0, \tag{8}$$

where σ_{Th} is the Thomson cross section [26], and L_0 writes

$$\begin{aligned} L_0 &\cong \frac{f}{2\pi} \frac{N_l N_e}{\Sigma_{e,l}}, \\ \Sigma_{e,l} &= \sigma_e^2 + \sigma_l^2, \end{aligned} \tag{9}$$

being σ_e the r.m.s. electron bunch transverse section, σ_l the r.m.s. laser beam transverse section and f the rate of the collisions. We have considered a round beam, otherwise $\Sigma_{e,l}$, should be replaced by $\sqrt{(\sigma_{e,x}^2 + \sigma_{l,x}^2)(\sigma_{e,y}^2 + \sigma_{l,y}^2)}$.

The previous relationships suggest the naïve, but importantly, consideration that the output flux is optimized by increasing the number of electrons, (and therefore the electron bunch charge) the number of photons (and thus the laser intensity) and finally by matching and minimizing the electron and laser transverse sections.

We can handle Equation (8) in order to obtain a more convenient form, for practical purposes. If we replace the number of electrons with the bunch charge divided by the electron elementary charge ($N_e = Q_e/e$) and the number of photons in the laser pulse as the laser energy divided by the single photon energy, we find from Equation (8)

$$\begin{aligned} \dot{N}_x &\cong kf \frac{\widetilde{E}_l \overline{Q}_e \lambda_l}{(1+d)}, \\ k &= \frac{8}{3} \pi \frac{r_0}{\hbar I_0}, \\ \overline{Q}_e &= \frac{Q_e}{2\pi \sigma_e^2} \equiv \text{electron beam charge density}, \\ \widetilde{E}_l &= N_l \mathcal{E}_l, \\ d &= \frac{\sigma_l^2}{\sigma_e^2}. \end{aligned} \tag{10}$$

It should be noted that in SI units k reads

$$k[m/JAs] = 1.317 \times 10^{16}. \tag{11}$$

As already underlined, the key parameters of our discussion are the bunch charge, the laser energy, the transverse cross sections of laser/electron bunches and the collision repetition frequency. Regarding the design strategy, we cannot define (at least on the basis of the elements provided so far) any effective optimization criteria, except that of keeping the largest values of Q_e, $\widetilde{E}_l$ and f and the smallest values of $\sigma_{e,l}$. Furthermore, regarding the collision frequency we note that the combined use of recirculated beams and of laser pulse stacking in high Q-cavities provides values exceeding the tens of MHz (for more details see Refs. [27,28]).

Albeit fairly elementary, what we have accomplished so far is sufficient to get preliminary indications regarding the working point of an X-ray CBS source. In order to operate in the hard X-ray region (7–8 KeV) with laser wavelength of 1 µm, an e-beam with 25 MeV energy is sufficient. In order to proceed we use Equation (10) to specify the amount of charge density to get a definite X-ray flux. If we assume that the laser and electron r.m.s. beam transverse sections are matched ($d \cong 1$), we find

$$\overline{Q}_e \cong \frac{2}{kf\,\widetilde{E}_l\,\lambda_l}\dot{N}_x. \tag{12}$$

In Table 1 we have reported the normalized emittance (ε_n), namely the electron beam phase space area at the cathode. The corresponding value when the beam is brought to relativistic energies is ε_n/γ. It should furthermore be noted that β_T (the Twiss parameter) and ε_n reported in the table refers to radial and vertical components.

Table 1. Reference Parameters for CBS X-ray Source.

$\dot{N}_x\,[s^{-1}]$	1.6×10^{14}
$f[Hz]$	10^8
$\widetilde{E}_l[J]$	10^{-2}
$\lambda_l[m]$	10^{-6}
γ	50
$\beta_T[m]$	5×10^{-3}
$\varepsilon_n[mm\ mrad]$	0.1

Furthermore, using for the other quantities on the r.h.s. of Equation (12) the values reported in Table 1 [29–32], we end up with $\overline{Q}_e\left[C/m^2\right] \cong 0.025$, which is a reasonable value, as we will see below.

Taking into account that the e-beam transverse sections are linked to emittance and beam parameters by the relationship

$$\sigma_e^2 = \beta_T \frac{\varepsilon_n}{\gamma}, \tag{13}$$

we can derive from Equation (12) the total charge as

$$Q_e \cong \frac{2}{kf\,\widetilde{E}_l\,\lambda_l} 2\pi \frac{\beta_T \varepsilon_n}{\gamma}\dot{N}_x. \tag{14}$$

The use of the parameters in Table 1 yields for the amount of the bunch charge $Q_e = 1.579\ pC$, consistent with the assumptions in ref. [29].

A key point, loosely mentioned in the previous discussion, is the striking request on the smallness of the electron and laser beam sections at the interaction point (IP). This can be realized by exploiting beams with small normalized emittance and small beta parameters. The realizations of these conditions pass through two bottlenecks: the design of an adequate RF gun producing an electron beam with a small emittance at the cathode and an extremely

challenging beam transport at the IP (see below for further comments). Within this respect, the parameters reported in Table 1 are challenging and are an example of the design paradigm, we mentioned before: the large collision rate, and the small transverse section area, achieved through a small normalized emittance of 0.1 *mm mrad* (a factor 10 below those used for the operation of SASE FEL linacs) and β_T (for both the x, y components) of 5 *mm*. Further details on the design of the electron gun foreseen to achieve the electron beam performances can be found in ref. [29].

Furthermore, introducing the electron bunch peak current using the definition

$$\hat{I}_e = \frac{Q_e}{\sqrt{2\pi}\sigma_\tau} \qquad \sigma_\tau \equiv \text{e- bunch duration}, \tag{15}$$

we find from Equation (14)

$$\hat{I}_e \cong \frac{2\sqrt{2\pi}}{kf\sigma_\tau \widetilde{E}_l \lambda_l} \frac{\beta_T \varepsilon_n}{\gamma} \dot{N}_x, \tag{16}$$

which links together the macroscopic parameters characterizing the whole device.

Furthermore, using the definition of beam power asa product of e-beam current and energy, we find from Equation (16) the following relation

$$\hat{P}_e[W] \cong \frac{1.944 \cdot 10^{-10}}{f\sigma_\tau \widetilde{E}_l \lambda_l} \beta_T \varepsilon_n \dot{N}_x, \tag{17}$$

which yields the beam power in terms of the X-ray photon flux.

Before concluding this introductory section it is worth mentioning some points relevant to the calculation of the brightness. To this aim, we remind the reader that

(a) For the photons emitted per 0.1% bandwidth (*bw*), we define (see Ref. [10])

$$\dot{N}_{x,0.1\%} = 1.5 \times 10^{-3} \dot{N}_x. \tag{18}$$

(b) For the range of parameters discussed in this paper, the backscattered X-ray beam is not "non-diffraction-limited", namely the normalized emittance does not satisfy the condition

$$4\pi\gamma\varepsilon_n < \lambda_l, \tag{19}$$

as it can be checked using the parameters in, e.g., Table 1

(c) For a non diffracted beam the brightness is defined as

$$B[s^{-1}/(mm\ mrad)^2/(0.1\%bw)] = \frac{\dot{N}_{x,0.1\%}\gamma^2}{4\pi^2 \varepsilon_{n,x}\varepsilon_{n,y}}. \tag{20}$$

The previous considerations are the 0-th-order tools to start any discussion on the "dimensioning" of a CBS X-ray source.

It is evident that, albeit reasonable, the present description misses non secondary features, to be considered reliable:

(i) The effect of electron and "optical" beams (laser and X-ray) longitudinal and transverse distributions.

(ii) The inhomogeneous broadening associated with e-beam energy spread and emittances.

In the following sections, we will see how the previous considerations, of pure common sense, can be corroborated by a more thoughtful model. We develop also a computational scheme to account for the interplay between electron beam qualities and CBS spectral details and we comment on its use for the design of an actual photon source.

2. Fixing a More Realistic Model

In this section we put the "theoretical frame" of the introductory section on a more firm basis, including the details associated with electron and laser beam distribution details.

The assumption underlying the definition of brightness in Equation (20) is that the laser spot envelopes the electron beam (see Figure 4). Furthermore, it implicitly contains the hypothesis that the transverse phase space angular divergence of the scattered X-rays matches that of the electron beam.

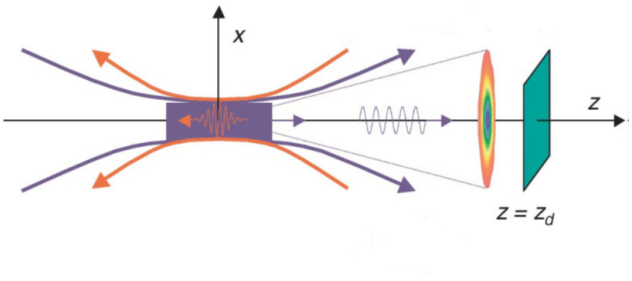

Figure 4. Laser and scattered X-ray beam longitudinal profiles. The screen in green represents the detector and z_d is the relevant longitudinal coordinate. (see Ref. [33] for further details).

In the numerical example presented in the previous section, we have assumed a large repetition rate, a small emittance and a very low β_T value at the IP.

We have accordingly followed a naïve optimization procedure, which simply maximizes the repetition rate and minimizes the laser and electron transverse dimension at IP. The electron bunch length should be furthermore sufficiently short to avoid the hour-glass effect, as understood by inspecting Figure 4.

The weakness of the discussion developed in the introductory section is displayed in Figure 4, where we have reported the CBS collision region, indicating the hour-glass effect associated with the incoming laser and output X-ray beam diffraction behavior [33]. Any reasonable model should therefore include the spatial and temporal dependence of the laser and electron distribution. Assuming a cylindrical symmetry we can write the number of photons scattered per unit volume and unit time as

$$\frac{d^3N_x}{c\,dVdt} = \sigma_{Th}(1+\beta_0)\tilde{N}_l(r,z,t)\tilde{N}_e(r,z,t), \tag{21}$$

with $dV = 2\pi r dr dz$ as the volume element in cylindrical coordinates, $\tilde{N}_{l,e}$ as the laser and electron number distribution and β_0 as the average electron on axis reduced velocity.

It is evident that Equation (21) is substantially equivalent to our starting Equation (8), with the only difference that, in order to evaluate the number of scattered X-photons, it is necessary to perform an integration on the transverse volume and on the longitudinal coordinate.

We will follow the indications in Ref. [33] to model the electron and laser photon distributions by the use of the same formalism. We exploit indeed the fact that the relevant longitudinal and transverse envelopes can be viewed as equivalent, if the transport is provided by linear optical elements (lens, quadrupoles, etcetera) where aberrations do not play any significant role [34,35]. We write therefore

$$\tilde{N}_p(r,z,t) = \frac{N_p}{A_p}\frac{1}{\sigma_p(z)^2}e^{-\frac{r^2}{\sigma_p(z)^2}}e^{-\frac{t_p(z)^2}{\Delta\tau_p^2}}, \tag{22}$$

$$p \equiv l, e.$$

The previous function is nothing but a Gaussian in time and transverse coordinate, the quantities $\sigma_p(z)$ and $\Delta\tau_p$ are the r.m.s. of the longitudinal and temporal distributions

and A_p is the normalization constant. The specific forms for the e/l dependence on z is given below

$$\sigma_e(z) = \sigma_e\sqrt{1+\left(\frac{z}{\beta_T}\right)^2},$$
$$\sigma_l(z) = \sigma_l\sqrt{1+\left(\frac{z}{Z_R}\right)^2}, \tag{23}$$

where σ_e, β_T are the already introduced electron-beam section and Twiss parameter, respectively. The laser section σ_l and Z_R are associated with the beam waist and Rayleigh length, namely

$$\sigma_l^2 = \frac{W_0^2}{2}, \quad W_0 \equiv \text{laser beam waist},$$
$$Z_R = \frac{\pi W_0^2}{\lambda_l}$$
$$A_e = \pi^{3/2} c\Delta\tau, \tag{24}$$
$$A_l = 2\left(\frac{\pi}{2}\right)^{3/2} c\Delta t.$$

In passing, we remind the reader of close analogy between the Rayleigh length and the β_T parameter [34–36]. We carry out the integration on the transverse coordinate, without specifying (see below) $t_p(z)$, we get therefore

$$\frac{d^2N_x}{c\,dtdz} = \frac{2\pi\sigma_{Th}N_lN_e(1+\beta_0)}{\sigma_l(z)^2\sigma_e(z)^2A_eA_l}e^{-\frac{t_l(z)^2+t_e(z)^2}{\Delta\tau^2}}\int_0^\infty e^{-\left[\frac{\sigma_e(z)^2+\sigma_l(z)^2}{\sigma_e(z)^2\sigma_l(z)^2}\right]r^2} rdr =$$
$$= \frac{\pi\sigma_{Th}(1+\beta_0)}{A_eA_l}\widetilde{L}_0(z),$$
$$\Delta\tau_e = \Delta\tau_l = \Delta\tau, \tag{25}$$
$$\widetilde{L}_0(z) = \frac{N_lN_e}{[\sigma_e(z)^2+\sigma_l(z)^2]}e^{-\frac{t_l(z)^2+t_e(z)^2}{\Delta\tau^2}}.$$

The superimposed tilde denotes the luminosity divided by the collision frequency, $\tilde{L}_0(z)$ is a function of the longitudinal coordinate and therefore

$$\frac{dN_x}{dt} = \frac{c\pi\sigma_{Th}(1+\beta_0)}{A_eA_l}\int_{-\infty}^{\infty}\tilde{L}_0(z)dz. \tag{26}$$

It is important to emphasize that dN_x/dt is not the photon flux $\dot{N}_x$ defined in the previous section. The derivative in Equation (26) refers to the microscopic time, while the superimposed "dot" accounts for the macroscopic time associated to the rate of collisions.

In order to perform the integration, it is necessary to carefully specify the dependence of the luminosity on the z-variable. We note therefore that

$$\begin{aligned} &\sigma_e(z)^2 + \sigma_l(z)^2 = (\sigma_l^2 + \sigma_e^2)(1+\zeta^2), \\ &\zeta = \kappa z, \\ &\kappa = \frac{1}{Z_R}\sqrt{\frac{1 + r_T^2 \frac{Z_R^2}{\beta_T^2}}{1 + r_T^2}}, \\ &r_T = \frac{\sigma_e}{\sigma_l}. \end{aligned} \tag{27}$$

Regarding the definition of $t_p(z)$, we note that an appropriate discussion, including the detector time (namely the time at which the X-ray flux is measured on a screen placed at $z = z_d$) has been developed in Ref. [33]. The definition of the laser and electron pulse time, t_l and t_e, are respectively reported in Ref. [33] is more general and comprises a fairly elaborated conceptual scheme, accounting for the current time t (namely that ruling the interaction at the IP) and the detector time t_d (namely the time at which the scattered photons are collected at z_d). Since we limit ourselves to the backscattering geometry we drop such a distinction and simply set

$$\begin{aligned} &t_e(z) = t, \\ &t_l(z) = 2\sqrt{2}\frac{z}{c}, \end{aligned} \tag{28}$$

where $2\sqrt{2}$ is just a matter of normalization, due to the definition of the laser pulse duration Δt, linked to the bandwidth as $\Delta\omega_l \Delta t = \sqrt{2}$.

Assuming the conditions of Equation (28) we get

$$\begin{aligned} &e^{-\left(\frac{t_l(z)}{\Delta t}\right)^2 - \left(\frac{t_e(z)}{\Delta \tau}\right)^2} = e^{-\left(\frac{t}{\Delta\tau}\right)^2} e^{-\chi\zeta^2}, \\ &\chi = \left(\frac{2\sqrt{2}}{c\Delta t \kappa}\right)^2, \quad \sigma_{z,e} = c\Delta t. \end{aligned} \tag{29}$$

We can therefore carry out the integration on the longitudinal coordinate z, thus getting from Equation (26)

$$\frac{dN_x}{dt} = \frac{2\pi^2 c \sigma_{Th}(1+\beta_0)}{A_e A_l \kappa}\frac{L_0}{f} e^{-\left(\frac{t}{\Delta\tau}\right)^2}\int_{-\infty}^{\infty}\frac{e^{-\chi\zeta^2}}{1+\zeta^2}d\zeta. \tag{30}$$

The use of the following integration procedure [37]

$$\begin{aligned} &\int_{-\infty}^{\infty}\frac{e^{-\chi\zeta^2}}{1+\zeta^2}d\zeta = \int_0^{\infty} e^{-s}\left[\int_{-\infty}^{\infty} e^{-(\chi+s)\zeta^2}d\zeta\right]ds = \\ &= \sqrt{\pi}\int_0^{\infty}\frac{e^{-s}}{\sqrt{\chi+s}}ds = e^{\chi}\sqrt{\pi}\Gamma\left(\frac{1}{2},\chi\right), \\ &\Gamma(\nu,a) \equiv \text{ Incomplete Gamma function,} \end{aligned} \tag{31}$$

eventually yields

$$\frac{dN_x}{dt} = \frac{\sigma_{Th} L_0}{f} \Phi e^{-\left(\frac{t}{\Delta\tau}\right)^2},$$
$$\Phi = \frac{2\pi^{5/2} c(1+\beta_0)}{A_e A_l \kappa} e^{\chi} \Gamma\left(\tfrac{1}{2}, \chi\right), \tag{32}$$
$$\kappa = \left(\frac{2\sqrt{2}}{\sigma_{z,e}\sqrt{\chi}}\right).$$

The function Φ marks the difference with respect to the results of the previous section (see Equation (8)). To appreciate its physical meaning, further algebraic manipulations are in order. We can, accordingly, introduce the flux function

$$\Phi = \frac{2}{\sqrt{\pi}\Delta\tau} \sqrt{\chi} e^{\chi} \Gamma\left(\frac{1}{2}, \chi\right),$$
$$\chi = \left(\frac{2\sqrt{2}}{c\Delta t \kappa}\right)^2 = 8 r_z^2 \left[\frac{Z_R}{\sigma_{z,e}} \sqrt{\frac{1+r_T^2}{1+r_T^2 \frac{Z_R^2}{\beta_T^2}}}\right]^2, \tag{33}$$
$$r_z = \left(\frac{\sigma_{z,e}}{\sigma_{z,l}}\right),$$

and if we integrate with respect to time, we obtain the number of scattered photons

$$N_x \cong 2\sigma_{Th} \frac{L_0}{f} F(\chi),$$
$$F(\chi) = \sqrt{\chi} e^{\chi} \Gamma\left(\frac{1}{2}, \chi\right). \tag{34}$$

The X-ray photon counting, including the rate of collisions, is therefore

$$\dot{N}_x \cong 2\sigma_{Th} L_0 F(\chi). \tag{35}$$

It is evident that the corrections to the result of Section 1 are essentially given by the function $F(\chi)$, depending on a single variable. The relevant behavior is reported in Figure 5. Even though an optimum in the strict sense does not exist for large values of χ, the function approaches values close to unit.

Choosing therefore $A \cong 1$ and $\chi \geq 10$ (compatible with effective experimental parameters [33]), we recover the starting point of Equation (8).

The main result of this section is that, even though naïve, the conclusions we have drawn in the introduction are consistent with the analysis developed here, which can be exploited for a more appropriate optimization of the whole device.

The forthcoming sections contain further elaboration including the spectral structure of the X-ray output beam and the relevant inhomogeneous broadening induced by the beam qualities.

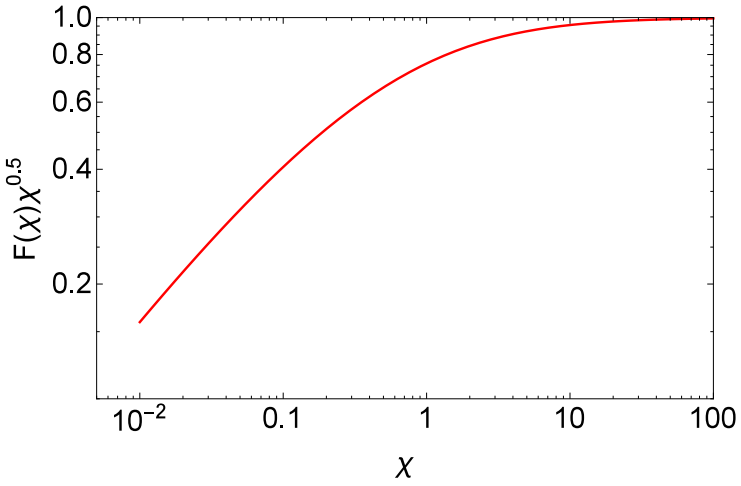

Figure 5. Log-log plot of the flux function $F(\chi)\sqrt{\chi}$.

3. Spectral Properties and Inhomogeneous Broadening

In the previous two sections we have not considered the spectral properties of the Thomson backscattering, which are affected by the structure of the electron beam itself and determine a dilution of the spectral brightness. Here we fix a simple procedure to account for the quoted effects.

Before going further, we take a step back and better clarify what we have already mentioned without any thorough discussion.

Regarding the definition of Thomson scattering limit of CBS, we note that it occurs if the electron recoil (see Figure 6) does not play any role in the scattering process, or, similarly, when the energy of scattered photons is negligible with respect to e-beam energy.

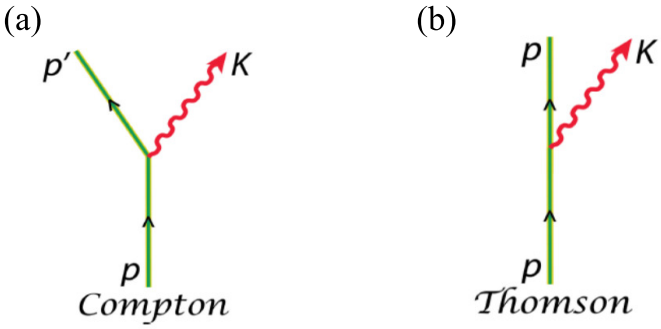

Figure 6. Vertex of the Feynman diagram expressing the difference between Compton (**a**) and Thomson Scattering (**b**). In case (**b**), the electron dynamics remain practically unperturbed after the interaction process.

Even though academic, for the range of parameters considered here, we will comment on the effect of quantum corrections to CBS in the final section.

As is well known [7], underscored in the introduction and discussed elsewhere in this issue [38], within this approximation, the CBS can be treated using the same procedure adopted to treat radiation emission in the magnetic undulator. The analogy allows a straightforward inclusion of the spectral inhomogeneous broadening and of the non-linear contributions, which occur at larger laser intensities. They are responsible for frequency shift (due to the laser equivalent strength parameter) and for inducing a figure eight-like motion in the electron trajectory, determining the emission at higher harmonics [39].

The energy of the scattered photons with the inclusion of the effect of the laser wave intensity and of small angular deviation from the head-on collision (see Figure 7) writes

$$\hbar\omega_s = \frac{4\gamma^2\hbar\omega_l}{1+\frac{K_l^2}{2}+(\gamma\vartheta)^2}. \tag{36}$$

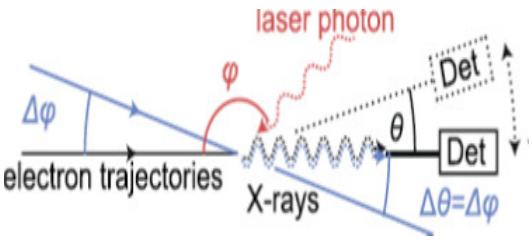

Figure 7. Geometry of the Compton Backscattering including angular shifts.

The previous equation refers to the wavelength scattered by a single electron, since the bunch is composed by electrons with different energies and different entrance angles, it will be necessary to evaluate the frequency shift associated with the deviations from the reference values and then make an average on the electron energy and angular distributions.

This procedure has been described in articles and textbooks (see [3,5,37,39–42] and references therein) and will not be repeated here. We just remind the reader that it is sufficient to evaluate the relative frequency shift, composed as

$$\begin{aligned} &\frac{\delta\omega}{\omega} = \left(\frac{\delta\omega}{\omega}\right)_{\varepsilon} + \left(\frac{\delta\omega}{\omega}\right)_{K_l} + \left(\frac{\delta\omega}{\omega}\right)_{\vartheta} \\ &\varepsilon = \frac{\delta\gamma}{\gamma} \equiv \text{relative energy deviation} \end{aligned} \tag{37}$$

where the different terms are due to deviation in energy (ε), laser strength parameter (K_l) and scattering angle (θ). The dependence of K_l on the transverse coordinate comes from the laser mode distribution shape, while the angular variables from the relation $\vartheta^2 = x'^2 + y'^2$.

Considering that the spectral shape is given by [34]

$$\begin{aligned} &S(\nu) = \left[\frac{\sin\left(\frac{\nu}{2}\right)}{\left(\frac{\nu}{2}\right)}\right]^2 = 2Re\left(\int_0^1 (1-t)e^{-i\nu t}dt\right), \\ &\nu = 2\pi\,\widetilde{N}_l\frac{\omega_x-\omega}{\omega_x}, \end{aligned} \tag{38}$$

where $\widetilde{N}_l = c\Delta T/\lambda_l$ is the number of laser cycles within the pulse duration.

The convolution on the electron beam distribution can be evaluated as

$$\begin{aligned} &\langle S(\nu)\rangle = \int_D S(\nu+\delta\nu)f(x,x';y,y';\varepsilon,t)d^5x, \\ &\delta\nu = 2\pi\,\widetilde{N}_l\frac{\delta\omega}{\omega}, \end{aligned} \tag{39}$$

where $f(x,x';y,y';\varepsilon,t)$ is the e-beam six dimensional phase-space distribution.

We assume that the distributions can be factorized as

$$f(x,x';y,y';\varepsilon,t) = F(x,x';y,y')\phi(\varepsilon)\phi(t) \tag{40}$$

where $F(x,x';y,y') = g(x,x')g(y,y')$, with

$$g(\eta,\eta') = \frac{1}{2\pi\varepsilon_\eta}\exp\left(-\frac{\gamma_\eta^2\eta^2 - 2\alpha_\eta\eta\eta' + \beta_\eta\eta'^2}{2\varepsilon_\eta}\right), \quad \eta = x,y \quad ,$$

$$\phi(\epsilon) = \frac{1}{\sqrt{2\pi}\sigma_\epsilon}\exp\left(-\frac{\varepsilon^2}{2\sigma_\epsilon^2}\right), \quad \epsilon = \frac{\gamma-\gamma_0}{\gamma_0}, \tag{41}$$

$$\phi(t) = \frac{1}{\sqrt{2\pi}\sigma_t}\exp\left(-\frac{t^2}{2\sigma_t^2}\right).$$

The normalization of the phase space $g(\eta,\eta')$ distribution is ensured if the Twiss parameters satisfy the condition [43]

$$\gamma_\eta\beta_\eta - \alpha_\eta^2 = 1. \tag{42}$$

The level curves of $g(\eta,\eta')$ can be exploited to visualize the geometrical content of Courant-Snyder invariant (see Figure 8), the rms values of the radial and vertical beam sections and of the angular divergences placed on the curve line in correspondence with the tangent points of the lines parallel to the axis η and η', respectively.

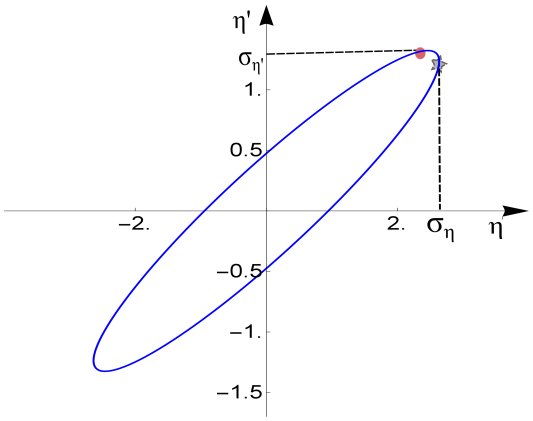

Figure 8. Courant-Snyder ellipse, $\gamma_\eta^2\eta^2 - 2\alpha_\eta\eta\eta' + \beta_\eta\eta'^2 = \epsilon_\eta$. The abscissa of the point denoted by a dot yields the rms of the e-beam angular divergence, the ordinate of the point denoted by a star yields the associated rms transverse section.

The technicality associated with the evaluation of the convolution integral is just a matter of working out multi-dimensional Gaussian integrals. The use of the integral representation on the r.h.s. of Equation (38) simplifies such a task and leads to an analytically manageable form, as reported below [34]

$$\langle S(\nu)\rangle = 2Re\int_0^\tau (1-t)\frac{e^{-i\nu t - \frac{1}{2}(\pi\mu_\varepsilon t)^2}}{\sqrt{R_x(t)R_y(t)}}\,dt,$$
$$R_\eta(t) = (1+\alpha_\eta^2)(1-\imath\pi\mu_\eta t)(1-\imath\pi\mu_{\eta'}t) - \alpha_\eta^2, \tag{43}$$

where we have included either the effects of the energy spread and emittances, which are specified through the inhomogeneous broadening parameters [34]

$$\begin{aligned}
&\mu_\varepsilon = 4\widetilde{N}_l\sigma_\varepsilon,\\
&\mu_{\eta'} = \frac{4\widetilde{N}_l\gamma^2\varepsilon_\eta}{\left(1+\frac{K_l^2}{2}\right)\beta_\eta};\quad \mu_\eta = \frac{4\,\widetilde{N}_l\gamma^2\varepsilon_\eta}{\left(1+\frac{K_l^2}{2}\right)\gamma_\eta}k_\beta^2,\\
&\varepsilon_\eta = \frac{\varepsilon_n}{\gamma};\quad \eta = x,y\ ,\\
&k_\beta = \frac{\pi K_l}{\gamma\lambda_l} \equiv \text{betatron motion wave number.}
\end{aligned} \tag{44}$$

Taking into account that

$$\sigma_{\eta'}^2 = \gamma_\eta\varepsilon_\eta,\ \ \sigma_\eta^2 = \beta_\eta\varepsilon_\eta, \tag{45}$$

we can also write

$$\begin{aligned}
&\mu_{\eta'} = \frac{4\widetilde{N}_l\gamma^2\sigma_{\eta'}^2}{\left(1+\frac{K_l^2}{2}\right)(1+\alpha_\eta^2)},\\
&\mu_\eta = \frac{4\widetilde{N}_l\gamma^2}{\left(1+\frac{K_l^2}{2}\right)(1+\alpha_\eta^2)}\left(\frac{\sigma_\eta}{\beta_T^*}\right)^2,\\
&\beta_T^* = k_\beta^{-1},
\end{aligned} \tag{46}$$

where β_T^* denotes the value of the Twiss parameter associated with the betatron wave number. The β_T^* is usually referred to as the undulator "natural" focusing parameter and, in absence of further focusing elements is the reference quantity for the electron beam matching.

It should be underlined that the optimization of the luminosity requires, as already noticed, extremely peculiar values of the Twiss coefficients at the IP. See Figure 9 where we have reported the bunch interaction at the overlapping point, where the β_T parameter of the electron beam is of the order of *cm* or even less.

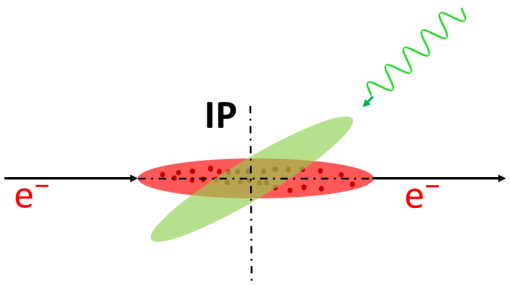

Figure 9. Geometry of the electron (red) and photon (green) bunches interaction at the IP.

If the e-beam is at waist in the crossing point, the γ_T parameters (inversely proportional to β_T) determine a significant increase of the e-beam divergence. It is therefore evident that the inhomogeneous broadening associated with the angular spread ($\mu_{\eta'}$) is dominant.

It should furthermore be noted that $\mu_\eta \propto K_l^2$ and therefore, to the laser intensity, for low I_l, the associated effect on the spectral broadening can be neglected.

To be less qualitative, we reconsider the definition of the laser equivalent strength parameter and note that

$$I_l\left[\frac{W}{m^2}\right] \cong 1.38 \times 10^{10} \frac{K_l^2}{\lambda[m]^2}. \tag{47}$$

Accordingly, for $K_l \cong 10^{-1}$ and using a laser wavelength 1 μm (a Ti: sapphire e.g.) the associated power density is $1.38 \times 10^{20}\ W/m^2$. For these values, the contribution of μ_η to the spectrum broadening can be neglected.

In Figures 10 and 11, we provide examples of spectrum distortion due to energy spread/"emittances" and Twiss parameters, respectively. The comments to the figures are summarized below

(i) Figure 10 yields an idea of the dependence of the spectral line on the energy spread. In the case of a symmetric energy distribution no spectral peak shift is exhibited and the most significant effects are the broadening and the reduction of the peak intensity.

(ii) Figure 11a displays the comparison between correlated and non correlated phase space e-beam distributions at the IP (see Figure 11b). A non-zero value of the $\alpha_{T(x,y)}$ correlation parameters determines an increase of the angular divergence along with a further broadening and an increase of the asymmetry and decreasing of the peak spectrum.

(iii) Figure 11c shows the comparison of the effect on the spectral line of the beam phase space distributions exhibiting different Twiss parameters (see Figure 11d). It is evident that either the spectral asymmetry and broadening are dominated by the effect of the larger angular divergence.

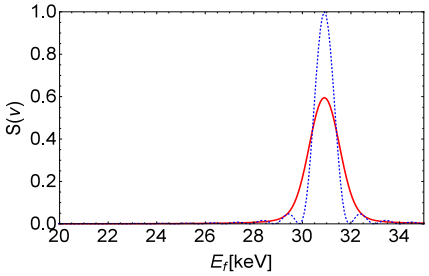

Figure 10. Spectral line of the scattered photons vs. energy (keV) for the e-beam and laser parameters $\lambda_l = 1$ μm, $\widetilde{N}_l = 100$, $\gamma = 100$ and for different values of energy spread and emittance; (continuous) $\sigma_\varepsilon = 2.5 \times 10^{-3}$, $\varepsilon_{n,x,y} = 0\ mrad$; (dot) $\sigma_\varepsilon = 0$, $\varepsilon_{n,x,y} = 0\ mrad$ (The value 0 means that the effect of the emittance has been considered negligible).

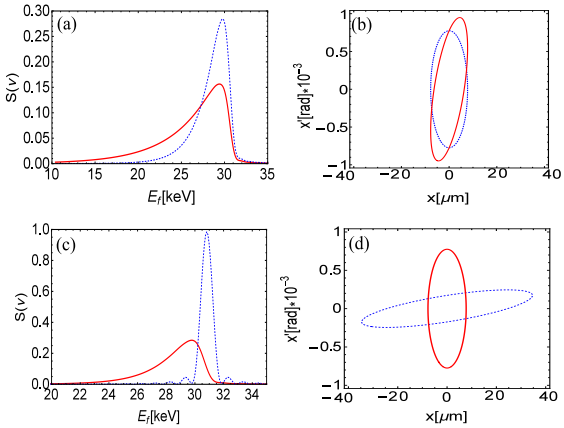

Figure 11. Spectral line of the scattered photons vs. energy (keV) (on the left) and the Courant-Snyder ellipse, respectively, (on the right) for the e-beam and laser parameters as Figure 10 with $\varepsilon_{n,x,y} = 3 \times 10^{-7}\ mrad$ and $\sigma_\varepsilon = 0$. Different combination of Twiss parameters has been provided; (**a**,**b**) $\beta_{T(x,y)} = 0.01\ m$, $\alpha_{T(x,y)} = 0.707$ (continuous), $\beta_{T(x,y)} = 0.01\ m$, $\alpha_{T(x,y)} = 0$ (dot); (**c**,**d**) $\beta_{T(x,y)} = 0.01\ m$, $\alpha_{T(x,y)} = 0$, (continuous), $\beta_{T(x,y)} = 0.2\ m$, $\alpha_{T(x,y)} = 1$ (dot).

The central peak frequency shift displayed by the cases with large $\gamma_{T(x,y)}$ is simply due to the fact that the e-beam divergences increase $\left(\langle\theta_{x,y}\rangle = \sqrt{\gamma_{T(x,y)}\varepsilon_{n,x,y}/\gamma}\right)$ and therefore the central peak frequency is given by

$$\omega^* \cong \frac{4\gamma^2\omega_l}{1+\frac{K_l^2}{2}+\left(\gamma\langle\theta_{x,y}\rangle\right)^2}. \tag{48}$$

In this section we have given a fairly simple picture of the distortion induced in the Thomson backscattering spectrum, by the electron beam qualities and by the relevant transverse phase-space distribution. The previous results compare fairly well with analogous (numerical) computations reported in ref. [42].

It is worth underlining that the use of a procedure yielding the full contribution to the spectral broadening, with the inclusion of the e-beam distribution in phase space is of noticeable importance. The necessity of squeezing the beam to get a larger photon flux is counteracted indeed by the insurgence of a large angular divergence, which hampers the spectral brightness; and therefore, an optimization procedure involving the beam transport design at the IP should carefully be accomplished. As a final remark we note that a small transverse section beam, like those reported here, demands an accurate analysis of the effects possibly induced by the Coulomb intra-beam scattering, which may eventually lead to an increase of the beam emittance and therefore to the deterioration of the spectral brightness. While not of crucial importance, but not fully secondary, this aspect of the problem will be treated elsewhere.

It should be noted that the spectral broadening we have considered here does not include the effect of the collimator [44], which will be discussed later in the section devoted to the final comments.

In the following section we will complete the analysis by including the effects associated with non-negligible values of the laser equivalent K-strength parameter.

4. Non Linear Contributions to Thomson Scattering

The increase of the laser intensity determines the increase of the associated K_l. As in the case of the magnetic undulator, a new and richer phenomenology arises, such as the possibility of extending the range of tunability through the emission of higher harmonics. In this section we will add a few comments on how these aspects of the CBS phenomenology should be accounted for.

As already noted, the wavelength shift due to the laser parameter K_l is one of these effects known since the early sixties of the last century [14]. The signature for the non-linear corrections is the emergence of a further broadening of the spectral line and the emission at higher order harmonics [7,14,28,38,39,44–50].

As previously underscored, the laser intensity effects can be quantified through the K_l parameter, using the analogy between the Thomson scattering and the emission in magnetic undulators. According to the present discussion, the undulator can be viewed as an ensemble of coherent photons, with a volumetric density [8]

$$\bar{n}_u \cong \frac{\alpha}{4}\frac{K_u^2}{\lambda_u r_0^2}, \tag{49}$$

providing a number of (virtual) photons, per cubic meter, of the order of 10^{29}. The use of Equations (8) and (49) allows to derive the number of scattered photons (the photon yield) by a single electron as reported below

$$N_s \cong c\Delta T\sigma_{th}\bar{n}_u = \frac{2}{3}\pi r_0^2 N_u K_u^2. \tag{50}$$

If we transpose the last identity to the case of the Thomson scattering, we naively infer that an increase of the laser intensity and therefore a corresponding increase of K_l, determines a significant enhancement of the scattered photons. This is not the only signature of the high intensity (non linear) regime.

If we pursue the analogy with the emission in undulators, we understand that with the increase of the output photon flux a richer phenomenology, including the appearance of higher order harmonics, becomes significant.

In order to address the problem of specifying, in less vague terms, the high field effects in Thomson backscattering, we use a more appropriate theoretical framework.

We remind the reader that the Lienard-Wiechert potentials yield the spectrum per unit solid angle as [7]

$$\begin{aligned}
&\frac{d^2 I_x}{d\omega d\Omega} = \sum_m \frac{d^2 I_{x,m}}{d\omega d\Omega} = \frac{16\,\alpha}{\pi} N_e \left(\gamma\,\widetilde{N}_l\right)^2 \xi_l^2 \sum_m m^2 f_{b,m}^2(\xi_l) \langle S_m(\nu_m)\rangle, \\
&\frac{d^2 I_{x,m}}{d\omega d\Omega} = \frac{16\,\alpha}{\pi} N_e \left(\gamma\,\widetilde{N}_l\right)^2 \xi_l^2 m^2 f_{b,m}^2(\xi_l) \langle S_m(\nu_m)\rangle, \\
&f_{b,m}(\xi_l) = (-1)^{\frac{m-1}{2}} \left[J_{\frac{m-1}{2}}(m\xi_l) - J_{\frac{m+1}{2}}(m\xi_l)\right],
\end{aligned} \tag{51}$$

where the sum is taken on the index of the harmonic m, $\langle S_m(\nu_m)\rangle$ is the same as in Equation (43), with the (significant) difference that the inhomogeneous broadening parameters are multiplied by the order of the harmonics and

$$\begin{aligned}
&\nu_m = 2\pi\left(m\,\widetilde{N}_l\right)\frac{\omega_{s,m}-\omega}{\omega_{s,m}}, \\
&\omega_{s,m} = m\omega_{s,1}, \;\; \omega_{s,1} = \omega_s.
\end{aligned} \tag{52}$$

It is evident that the spectrum distortion effects are more significant for higher harmonics. This is easily understood, since the μ parameters are the ratio between the induced homogeneous to the natural broadening and the latter is reduced by a factor m in the case of the higher order harmonics. We are now ready to start a more complete discussion.

The harmonic spectrum in Equation (51) is relevant to the radiation emitted on axis (even though it contains the angular corrections associated with the electron beam divergences).

In Figure 12, we have reported the quantity

$$A_m = \frac{\pi}{16\alpha N_e \left(\gamma\,\widetilde{N}_l\right)^2}\frac{d^2 I_{x,m}}{d\omega d\Omega} \tag{53}$$

and the relevant comments are reported below.

In Figure 12a, we have reported A_1 for large ($K_l = 1$) intensities. It is evident that, apart from the shift of the central peak when K_l increases, the most remarkable effect is the dominance of the line broadening and of asymmetry associated with the increase of the role of the spatial part of the transverse inhomogeneous broadening parameters (namely μ_η). Furthermore, these effects are even more significant for the spectral characteristics of higher harmonics (see Figure 12b).

Regarding the Equation (50), it should be noted that if we perform the evaluation of the number of emitted photons, we find after an integration over the frequency and solid angle the following result (see also ref. [45]) (obtained after a series expansion of the Bessel functions)

$$N_s \cong \frac{8}{3}\pi r_0^2 \widetilde{N}_l \xi_l \left[1 - \frac{8}{5}\xi_l + \frac{44}{35}\xi_l^2 \dots\right],$$
$$\xi_l = \frac{1}{4}\frac{K_l^2}{1+\frac{K_l^2}{2}}. \tag{54}$$

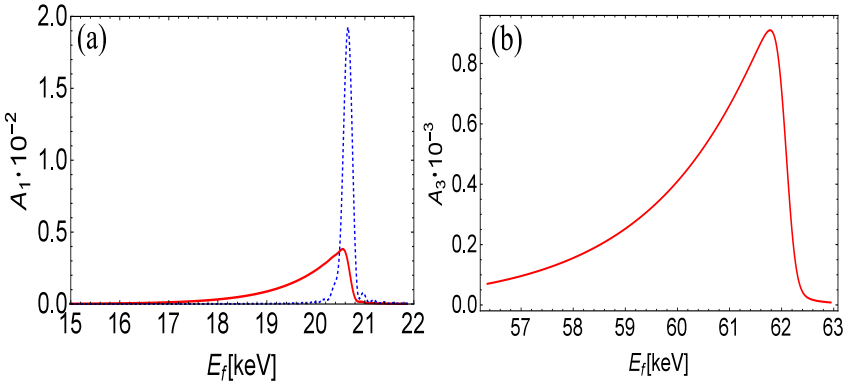

Figure 12. (**a**) A_1 vs. photon Energy, $\varepsilon_{n,x,y} = 3 \times 10^{-7} m \cdot rad$, $\sigma_\varepsilon = 2.5 \times 10^{-5}$, $\lambda_l = 1$ µm, $\widetilde{N}_l = 100$, $K_l = 1$, $n = 1$, $\beta_{T(x,y)} = 0.05\ m$, $\gamma_{T(x,y)} = 20\ m^{-1}$, $\alpha_{T(x,y)} = 0$ (continuous), $\beta_{T(x,y)} = 0.2$, $\gamma_{T(x,y)} = 5\ m^{-1}$, $\alpha_{T(x,y)} = 0$ (dot). (**b**) A_3 vs. photon Energy $\beta_{T(x,y)} = 0.05\ m$, $\gamma_{T(x,y)} = 20\ m^{-1}$, $\alpha_{T(x,y)} = 0$, $n = 3$.

This result is less naive than it may appear. It can indeed be interpreted as an intensity correction to the Thomson cross section, which, in terms of the parameter K_l, can be written as

$$\sigma_{th}(K_l) = \sigma_{th}\left[1 - \frac{7}{5}K_l^2 + \frac{263}{140}K_l^4 \dots\right]. \tag{55}$$

This opens new elements of discussion, which will be developed in the forthcoming section.

5. Final Comments

We have neglected, so far, quantum effects in the study of CBS. We have mentioned that most of our assumption is due to the neglecting of quantum recoil. The interplay between classical and quantum regimes is not as sharp as we have indicated. Some comments in this direction are addressed in this section.

In the previous sections, we have developed and summarized different ideas concerning the physics and the phenomenological aspects of the CBS, finalized to the design and construction of quasi-coherent X-ray sources.

We have underscored that the relevant theoretical and technological foundations deepen their roots in the research developed since the second half of the last century. In particular the underlying technology is the result of the tremendous effort aimed at providing high-intensity lasers. It is therefore important to emphasize that the breakthrough occurred with the introduction of the Chirped Pulse Amplification technique [51], and accelerators and high-quality beams. Within the last context, a not secondary role has been played by the development of FEL sources in all its declinations (oscillators, SASE, fourth generation of synchrotron radiation sources, etcetera).

We have underlined that, if the quantum effects are neglected, most of the formalism resembles that already exploited to understand the details of the radiation emitted in magnetic undulators [52,53]. This is however a superficial statement, which should be commented on more carefully.

To frame the problem in easily understandable physical terms, we list a few guiding parameters [54]

$$\psi = \frac{eE_l\lambda\!\!\!^{-}_e}{m_e c^2} = \frac{E_l}{\mathcal{E}_{ss}},$$
$$\varsigma = \frac{\hbar\omega_l}{m_e c^2} = \frac{\lambda\!\!\!^{-}_e}{\lambda\!\!\!^{-}_l}, \tag{56}$$
$$\mathcal{E}_{ss} = \frac{m_e c^2}{e}\frac{1}{\lambda\!\!\!^{-}_e} \cong 1.323 \times 10^{18} V/m,$$

where $\mathcal{E}_{ss}$ is the Sauter-Schwinger critical field [54,55], corresponding to the threshold energy for the creation of an $e^{\pm}$ pair.

The quantities ψ, ς compare, to the electron mass, the energy gained by an electron under the effect of an external field in a reduced Compton wavelength and the energy of a single laser photon, respectively.

Regarding the parameter ς, we note that it is hidden in Equation (1), which, in the limits of negligible angular and intensity dependent shift, yields the following scattered frequency and wavelength shift

$$\omega_s \cong \frac{4\gamma^2\omega_l}{1+4\gamma\varsigma},$$
$$\frac{\Delta\lambda_s}{\lambda_s} = 4\gamma\varsigma. \tag{57}$$

According to Figure 13a, we get that deviations from the classical limit can be observed for $4\gamma\varsigma > 0.1$, which can also be written as

$$\lambda_e > 2.5 \times 10^{-2}\frac{\lambda_l}{\gamma}, \tag{58}$$

quantum shift effects can, e.g., be observed for energies above 5 GeV for a pump laser with $\lambda_l \cong 500\ nm$ (2.48 eV) [56].

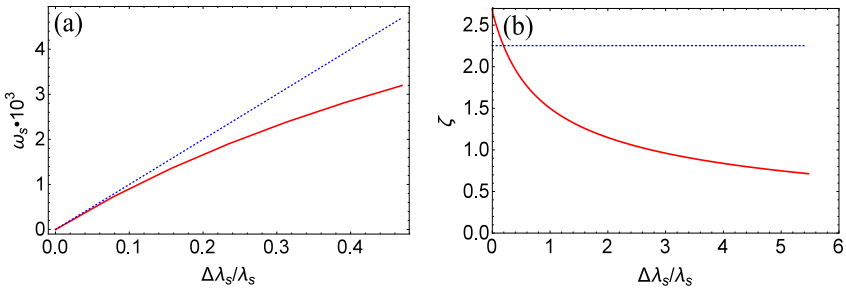

Figure 13. (**a**) Comparison between back-scattered photon frequency vs. $\Delta\lambda_s/\lambda_s$ with (dot) and without (continuous) recoil contributions. (**b**) CBS cross section normalized to πr_0^2 vs. $\Delta\lambda_s/\lambda_s$.

The same conclusion can be achieved by inspecting the CBS cross section vs. $4\gamma\varsigma$ reported in Figure 13b, which exhibits deviations larger than 10% with respect to the Thomson cross section for the same amount of $4\gamma\varsigma$.

According to the previous discussion, significant quantum effects can be observed in the process of X-ray photons scattered by energetic electrons. This problem has been addressed in Ref. [55,57], where the use of FEL X-ray beams to generate narrow band GeV photons via the backscattering of a 7 GeV electron beam has been proposed. In Figure 14, we have reported the differential cross section of the Compton backscattering of a pump laser with different photon energies (from IR to hard X-ray), namely

$$\frac{d\sigma}{d\varepsilon_2} \quad vs. \quad \varepsilon_2,$$

$$0 < \varepsilon_2 < \varepsilon_{\max}, \tag{59}$$

$$\varepsilon_{\max} = \frac{4\gamma^2\varepsilon_1}{1+4\gamma\varepsilon_1}, \quad \varepsilon = \frac{\hbar\omega}{m_e c^2}.$$

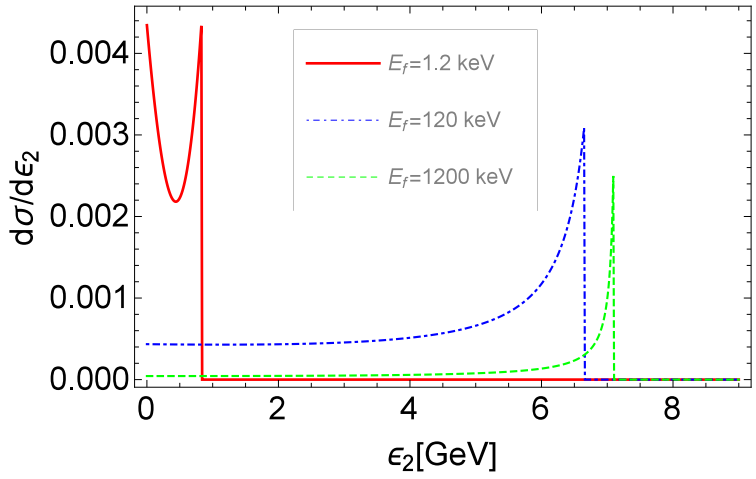

Figure 14. CBS differential cross section vs. ε_2 (given in GeV) for different energies of the laser pump (1.2 eV (continuous), 120 eV (dot-dash), 1200 keV (dash)).

Going back to ψ and ς, we note that they are quantum parameters, but their ratio defines the laser strength equivalent parameter, namely

$$K_l = \frac{\psi}{\varsigma}. \tag{60}$$

If we combine Equation (60) with the second of Equation (57), we end up with the following relationship

$$\frac{\Delta\omega_s}{\omega_s} = 4\frac{\gamma}{\sqrt{1+\frac{K_l^2}{2}}}\frac{\psi}{K_l}, \tag{61}$$

which is a "measure" of the quantum frequency shift in terms of the electric field size, energy and laser strength parameter, having included also the effect of the transverse motion in the definition of the relativistic factor (see Equation (4)).

Equation (61) is useful to specify different region of interest regarding the relative weight of quantum or non-linear intensity effects in the CBS process (see Figure 15 and Ref. [54]).

According to the Equation (56), $\psi = 1$ corresponds to the Sauter-Schwinger critical field yielding the creation of an $e^{\pm}$ pair [54,55].

In Figure 15a, we have reported $\Delta\omega_s/\omega_s$ vs. K_l for different values of ψ. In correspondence with $\psi = 1$, the laser electric field is equivalent to $\mathcal{E}_{ss}$, for lower values the insurgence of quantum effects becomes less significant. We have also marked the regions specifying the different regimes (Thomson, Compton, linear and non-linear). In Figure 15b, we have shown a comparison with the chart reported in Ref. [58], reporting the different zones of interest and the historical evolution in terms of laser power (hence of K_l), allowing the experimental benchmarking of these regimes.

It should be noted that Figure 15a has been drawn for $\gamma = 100$; for larger values, the lines are shifted towards larger quantum shifts values, thus allowing the access to the quantum regime with lower K_l values.

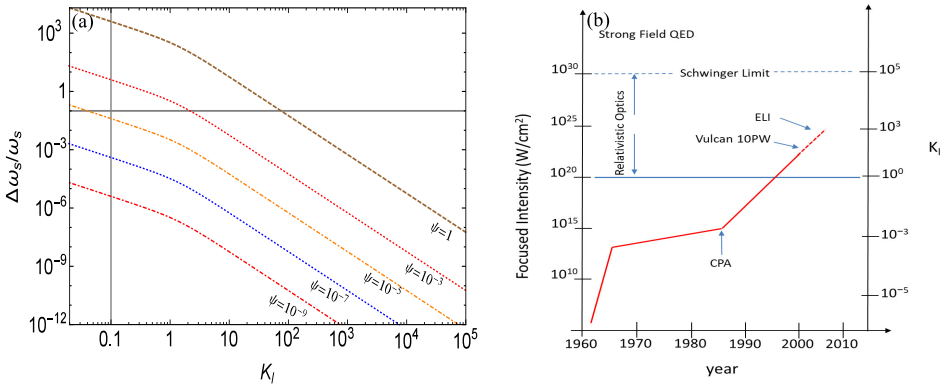

Figure 15. (**a**) Log-Log plot of $\Delta\omega_s/\omega_s$ vs. K_l for different values of ψ and $\gamma = 100$. The line $K_l = 0.1$ is the ideal separation of the linear regime ($K_l < 1$) from the non-linear regime ($K_l > 1$). The line $\Delta\omega_s/\omega_s = 0.1$ separates the Compton regime ($\Delta\omega_s/\omega_s > 0.1$) from the Thomson regime ($\Delta\omega_s/\omega_s < 0.1$). (**b**) Correspondence with the chart (adapted form Ref. [58]) regarding the evolution of high power lasers including also the historical evolution of light power laser technology. The knee marked with CPA is the breakthrough due to the introduction Chirped Pulse Amplification technique.

We have commented on the possibility of dealing with quantum effects in CBS scattering, but it is evident that can they be hardly detected in X-ray source devices. Most of the relevant effect is observed in higher energy photon scattering, which opens a so reach phenomenology and new effects in non linear QED [47–50,54,55,57], requiring a more appropriate and thorough discussion, for which there is not time in the present context.

Before concluding, we like to comment further on the CBS spectral broadening. We remind the reader therefore that, collecting the scattering photons on a suitably collimated angle, a narrow band or nearly mono-chromatic beam could be available, as a consequence of the restriction of photons at larger angles and therefore at larger wavelengths. However, the spatial, angular and energetic distribution of the electrons introduce the broadening, which combines with the bandwidth associated with the collimator. For this reason the total spectral bandwidth will be provided by

$$\left(\frac{\Delta\omega}{\omega}\right)_T = \frac{1}{2\widetilde{N}_l}\sqrt{1+\mu_\varepsilon^2+\mu_x^2+\mu_y^2+\mu_{x'}^2+\mu_{y'}^2+\mu_c^2}, \tag{62}$$

where [44]

$$\mu_c = \frac{\widetilde{N}_l}{\sqrt{3}}\frac{(\gamma\Phi)^2}{1+(\gamma\Phi)^2}, \tag{63}$$

is the broadening induced by the collimator with an angular acceptance Φ. It is evident that a large detection angle implies either a broadened spectral bandwidth or a larger number of collected photons. A general criterion to find a compromise, compatible with a specific application, between the two options is that of choosing

$$\mu_c^2 \cong \mu_\varepsilon^2+\mu_x^2+\mu_y^2+\mu_{x'}^2+\mu_{y'}^2. \tag{64}$$

For further comments on the problem of line broadening the reader is addressed to [42].

In this article, we have introduced a number of tools useful for the design of CBS X-ray sources, we have provided comments on the different regimes of operation, including strong field and we touched on quantum corrections. In a forthcoming investigation we will discuss different architecture for the design of X-ray CBS sources, including intra-cavity FEL photon backscattering [59].

Before concluding this review article, we would like to mention that the possibilities offered by the studies developed in the past on undulators with non standard configurations suggest possible extensions to "exotic" CBS. For example, the proposal of undulators with

two different periods (and different polarizations, as well) Refs. [60–63] has inspired the research program summarized in Ref. [64]. An analogous effort can be put forth using more advanced suggestions, as the proposal in Ref. [65] or the case of bi-hrmonic undulators [66], which, if transferred to CBS with appropriate laser configurations, offer a tool to enhance the associated harmonic emission in the strong field regime.

Author Contributions: Validation, G.D., E.D.P. and V.P.; Formal analysis, G.D., E.D.P. and V.P.; Investigation, G.D., E.D.P. and V.P. These authors contributed equally to this work. All authors have read and agreed to the published version of the manuscript.

Funding: This research received no external funding.

Institutional Review Board Statement: Not applicable.

Informed Consent Statement: Not applicable.

Data Availability Statement: Not applicable.

Acknowledgments: One of the Authors GD expresses sincere appreciation to S. Dabagov and to I. Drebot for an interesting post seminar discussion.

Conflicts of Interest: The authors declare no conflict of interest.

Nomenclature

The following abbreviations are used in this manuscript:

$\beta = v/c$	Reduced velocity, with v the electron velocity and c the speed of light
γ	Electron relativistic factor
λ_l	Laser wavelength
$\omega_l = \frac{2\pi c}{\lambda_l}$	Laser angular frequency
m_e	Electron mass
$\hbar$	Plank constant
$\lambda\!\!\!^{-}_c = \hbar/(m_e c)$	Reduced electron Compton wavelength
$\mathcal{E}_l = \hbar\omega_l$	Energy of a single photon laser
$\widetilde{E}_l$	Laser energy
K_l	Laser field strength parameter
N_l	Number of photons in a laser pulse
$\widetilde{N}_l$	number of laser cycles within the pulse duration
$E_e = m_e\gamma\, c^2$	Electron energy
B	Amplitude of the on axes magnetic field undulator
λ_u	Spatial period of the magnetic undulator
$K_u = \frac{eB\lambda_u}{2\pi\, m_e c}$	Strength parameter of a magnetic undulator
$r_0 = \frac{e^2}{4\pi\varepsilon_0 mc^2}$	Electron classical radius
$\sigma_{Th} = \frac{8}{3}\pi\, r_0^2$	Thomson cross section
$2\pi\sigma_e^2$	Electron beam transverse area
$I_0 = \frac{ec}{r_0} \cong 1.7 \times 10^4 A$	Alfvèn current
$\beta_{T(x,y)}$,$\alpha_{T(x,y)}$, $\gamma_{T(x,y)}$	β, α, γ Twiss parameter components in the transverse plane
RF Gun	Radio Frequency Gun
$\hbar = 6.62607015 \times 10^{-34}\ m^2 kg/s$	Plank constant

References

1. Madey, J.M. Stimulated emission of bremsstrahlung in a periodic magnetic field. *J. Appl. Phys.* **1971**, *42*, 1906–1913. [CrossRef]
2. Hajima, R. Status and Perspectives of Compton Sources. *Phys. Procedia* **2016**, *84*, 35–39. [CrossRef]
3. Dattoli, G.; Letardi, T.; Madey, J.; Renieri, A. Lawson-Penner limit and single passage free electron lasers performances. *IEEE J. Quantum Electron.* **1984**, *20*, 35–39. [CrossRef]

4. Dattoli, G.; Ottaviani, P.L.; Pagnutti, S. Booklet of FEL Design. 2007. Available online: http://fel.enea.it/booklet/pdf/Booklet_for_FEL_design.pdf (accessed on 27 June 2016).
5. Xie, M. Design optimization for an X-ray free electron laser driven by SLAC linac. *Proc. Part. Accel. Conf.* **1995**, *1*, 183–185. [CrossRef]
6. Ghaith, A.; Couprie, M.-E.; Oumbarek-Espinos, D.; Andriyash, I.A.; Massimo, F.; Clarke, J.A.; Courthold, M.; Bayliss, V.; Bernhard, A.; Trunk, M.; et al. Undulator design for a laser-plasma-based free-electron-laser. *Phys. Rep.* **2021**, *937*, 1–73. [CrossRef]
7. Esarey, E.; Ride, S.K.; Sprangle, P. Nonlinear Thomson scattering of intense laser pulses from beams and plasmas. *Phys. Rev. E* **1993**, *48*, 3003–3021. [CrossRef]
8. Dattoli, G.; Renieri, A. Experimental and theoretical aspects of the free-electron laser. In *Volume IV, Chapter in Laser Handbook*; Stitch, M.L., Ball, M.S., Eds.; North-Holland: Amsterdam, The Netherlands, 1985. [CrossRef]
9. Dattoli, G.; Gallardo, J.; Renieri, A.; Torre, A. Comment on "Photon antibunching in a free-electron laser". *Phys. Rev. A* **1985**, *32*, 3134. [CrossRef]
10. Krafft, G.A.; Priebe, G. Compton Sources of Electromagnetic Radiation, Reviews of Accelerator Science and Technology. *Rev. Accel. Sci. Technol.* **1985**, *3*, 147–163. [CrossRef]
11. Fermi, E. On the theory of collision between atoms and electrically charged particles. *Z. Phys.* **1924**, *29*, 315–327. [CrossRef]
12. Weizsäcker, C.F.V. Emission of very fast electrons collisions. *Z. Phys.* **1934**, *88*, 612–625. [CrossRef]
13. Williams, E.J. Nature of the High Energy Particles of Penetrating Radiation and Status of Ionization and Radiation Formulae. *Phys. Rev.* **1934**, *45*, 29–730. [CrossRef]
14. Milburn, R.H. Electron Scattering by an Intense Polarized Photon Field. *Phys. Rev. Lett.* **1963**, *10*, 75. [CrossRef]
15. Fiocco, G.; Thompson, E. Thomson Scattering of Optical Radiation from an Electron Beam. *Phys. Rev. Lett.* **1963**, *10*, 89–91. [CrossRef]
16. Nikishov, A.I.; Ritus, V.I. Quantum Processes in the Field of a Plane Electromagnetic Wave and in a Constant Field I. *Sov. Phys. JETP* **1964**, *19*, 529–541. Translated from *JETP* **1963**, *46*, 776–796.
17. Narozhny, N.B.; Nikishov, A.I.; Ritus, V.I. Quantum Processes in the Field of a Circularly Polarized Electromagnetic Wave. *Sov. Phys. JETP* **1965**, *20*, 622–629. Translated from *JETP* **1964**, *47*, 930–940.
18. Nikishov, A.I.; Ritus, V.I. Quantum Processes in the Field of a Plane Electromagnetic Wave and in a Constant Field II. *Sov. Phys. JETP* **1964**, *19*, 1191–1199. Translated from *JETP* **1964**, *46*, 1768–1781.
19. Brown, L.S.; Kibble, T.W.B. Interaction of Intense Laser Beams with Electrons. *Phys. Rev.* **1964**, *133*, A705–A719. [CrossRef]
20. Kibble, T.W.B. Frequency Shift in High-Intensity Compton Scattering. *Phys. Rev.* **1965**, *138*, B740–B753. [CrossRef]
21. Kibble, T.W.B. Refraction of Electron Beams by Intense Electromagnetic Waves. *Phys. Rev.* **1966** *16*, 1054–1056. [CrossRef]
22. Kibble, T.W.B. Mutual Refraction of Electrons and Photons. *Phys. Rev.* **1966**, *150*, 1060–1069. [CrossRef]
23. Reiss, H.R.; Eberly, J.H. Green's Function in Intense-Field Electrodynamics. *Phys. Rev.* **1966**, *151*, 1058–1066. [CrossRef]
24. Sarachik, E.S.; Schappert, G.T. Classical Theory of the Scattering of Intense Laser Radiation by Free Electrons. *Phys. Rev. D* **1970**, *1*, 2738–2753. [CrossRef]
25. Dattoli, G.; Nguyen, F. Free electron laser and fundamental physics. *Prog. Part. Nucl. Phys.* **2018**, *99*, 1–28. [CrossRef]
26. Jackson, J.D. *Classical Electrodynamics*, 3rd ed.; John Whiley and Sons Inc.: Hoboken, NJ, USA, 1999.
27. Hornberger, B.; Kasahara, J.; Gifford, M.; Ruth, R.; Loewen, R. A compact light source providing high-flux, quasi-monochromatic, tunable X-rays in the laboratory. In *Advances in Laboratory-based X-ray Sources, Optics, and Applications VII*; SPIE Publisher: Bellingham, WA, USA, 2019; Volume 1, p. 1111003. [CrossRef]
28. Petrillo, V.; Bacci, A.; Drebot, I.; Opromolla, M.; Rossi, A.R.; Rossetti, Conti, M.; Ruijter, M.; Samsam, S.; Serafini, L. Synchronised TeraHertz Radiation and Soft X-rays Produced in a FEL Oscillator. *Appl. Sci.* **2022**, *12*, 8341. [CrossRef]
29. Deitrick, K.; Delayen, J.R.; Gamage, B.R.P.; Hern, ez, K.; Hopper, C.; Krafft, G.A.; Olave, R.; Satogata, T. The ODU CAS Inverse Compton Source Design. Available online: http://toddsatogata.net/Papers/2013-09-03-ComptonSource-2up.pdf (accessed on 5 September 2013).
30. Krafft, G.A. ; Johnson, E.; Deitrick, K.; Terzić, B.; Kelmar, R.; Hodges, T.; Melnitchouk, W.; Delayen, J.R. Laser pulsing in linear Compton scattering. *Phys. Rev. Accel. Beams* **2016**, *19*, 121302. [CrossRef]
31. Deitrick, K. Inverse Compton Light Source: A Compact Design Proposal. Ph.D. Thesis, Old Dominion University, Norfolk, VA, USA, 2017. Available online: https://digitalcommons.odu.edu/physics_etds/7/ (accessed on 1 May 2017).
32. Deitrick, K.E.; Krafft, G.A.; Terzić, B.; Delayen, J.R. High-brilliance, high-flux compact inverse Compton light source. *Phys. Rev. Accel. Beams* **2018**, *21*, 080703. [CrossRef]
33. Hartemann, F.V.; Brown, W.J.; Gibson, D.J.; Anderson, S.G.; Tremaine, A.M.; Springer, P.T.; Wootton, A.J.; Hartouni, E.P.; Barty, C.P.J. High-energy scaling of Compton scattering light sources. *Phys. Rev. Accel. Beams* **2005**, *21*, 100702. [CrossRef]
34. Dattoli, G.; Renieri, A.; Torre, A. *Lectures on the Theory Free Electron Laser Theory and Related Topics*; World Scientific: Singapore, 1993.
35. Dattoli, G.; Doria, A.; Sabia, E.; Artioli, M.; *Charged Beam Dynamics, Particle Accelerators and Free Electron Lasers*; IOP Publishing Inc.: Philadelphia, PA, USA, 2017.
36. Rosenzweig, J.B. *Fundamentals of Beam Physics*; Oxford University Press: Oxford, UK, 2003.
37. Babusci, D.; Dattoli, G.; Licciardi, S.; Sabia, E. *Mathematical Methods for Physicists*; World Scientific: Singapore, 2019.
38. Di Palma, E.; Dattoli, G.; Sabchevski, S. Comments on the Physics of Microwave-Undulators. *Appl. Sci.* **2022**, *12*, 10297. [CrossRef]

39. Petrillo, V.; Bacci, A.; Ben Alì Zinati, R.; Chaikovska, I.; Curatolo, C.; Ferrario, M.; Maroli, C.; Ronsivalle, C.; Rossi, A.R.; Serafini, L.; et al. Photon flux and spectrum of γ-rays Compton sources. *Nucl. Instrum. Methods Phys. Res. Sect. A* **2012**, *693*, 109–116. [CrossRef]
40. Colson, W.B.; Gallardo, J.C.; Bosco, P.M. Free-electron-laser gain degradation and electron-beam quality. *Phys. Rev. A* **1986**, *34*, 4875–4881. [CrossRef]
41. Saldin, D.E.; Schneidmiller, E.V.; Yurkov, M.V. *The Physics of Free Electron Lasers*; Springer: Berlin/Heidelberg, Germany, 2000. [CrossRef]
42. Krämer, J.M.; Jochmann, A.; Budde, M.; Bussmann, M.; Couperus, J.P.; Cowan, T E.; Debus, A.; Köhler, A.; Kuntzsch, M.; García, A.L.; et al. Making spectral shape measurements in inverse Compton scattering a tool for advanced diagnostic applications. *Sci. Rep.* **2018**, *8*, 1398. [CrossRef] [PubMed]
43. Courant, E.D.; Snyder, H.S. Theory of the alternating-gradient synchrotron, *Ann. Phys.* **1958**, 3, 1646648–1646651. [CrossRef]
44. Hajima, R. Bandwidth of a Compton radiation source with an electron beam of asymmetric emittance. *Nucl. Instrum. Methods Phys. Res. Sect. A* **2021**, *985*, 164655. [CrossRef]
45. Zhao, S.; Lv, Q.; Yuan, S.; Li, Y. Surpassing one X-ray photon per electron in nonlinear Thomson scattering in 180 geometry. *Phys. Plasmas* **2012**, *19*, 01311. [CrossRef]
46. Harvey, C.; Heinzl, T.; Ilderton, A.; Marklund, M. Intensity-Dependent Electron Mass Shift in a Laser Field: Existence, Universality, and Detection. *Phys. Rev. Lett.* **2022**, *109*, 100402. [CrossRef]
47. Boca, M.; Florescu, V. Nonlinear Compton scattering with a laser pulse. *Phys. Rev. A* **2009**, *80*, 053403. [CrossRef]
48. Mackenroth, K.F. *Quantum Radiation in Ultra-Intense Laser Pulses*; Springer International Publishing: Cham, Switzerland, 2014.
49. Krajewska, K.; Kamiński, J.Z. Breit-Wheeler process in intense short laser pulsese. *Phys. Rev. A* **2012**, *86*, 052104. [CrossRef]
50. He, F.; Lau, Y.Y.; Umstadter, D.P.; Kowalczyk, R. Backscattering of an Intense Laser Beam by an Electron. *Phys. Rev. Lett.* **2003**, *90*, 055002. [CrossRef]
51. Strickl, ; D.; Mourou, G. Compression of amplified chirped optical pulses. *Opt. Commun.* **1985**, *55*, 447–449; Erratum: *Opt. Commun.* **1985**, *56*, 219–221. [CrossRef]
52. Alferov, D.F.; Bashmakov, Yu, A.; Bessonov, E.G. Undulator Radiation. In Proceedings of the Synchrotron Radiation And Free Electron Lasers, Grenoble, France, 22–27 April 1996; Basov, N.G., Ed.; P. N. Lebedev Physics Institute: Moscow, Russia, 1976; Volume 80, pp. 97–123.
53. Krisky, S.; Perlman, M.L.; Watson, R.E. Characteristics of Synchrotron Radiation and of Its Sources. In *Handbook of Synchrotron Radiation*; Eckhard Koch, E., Ed.; North Holland Publishing Company: Amsterdam, The Netherlands, 1983; pp. 65–171.
54. Heinz, T. QED and Lasers: A Tutorial. *arXiv* **2022**, arXiv:2203.01245v1.
55. McDonald, K.T. Proposal for Experimental Studies of Nonlinear Quantum Electrodynamics. Princeton Preprint DOE-ER-3072-38 (Unpublished). Available online: http://kirkmcd.princeton.edu/e144/prop.pdf (accessed on 2 September 1986).
56. An, G.-P.; Chi, Y.-L.; Dang, Y.-L.; Fu, G.-Y.; Guo, B.; Huang, Y.-S.; He, C.-Y.; Kong, X.-C.; Lan, X.-F.; Li, J-C.; et al. High energy and high brightness laser compton backscattering gamma-ray source at IHEP. *Matter Radiat. Extrem.* **2018**, *3*, 219–226. [CrossRef]
57. Bamber, C.; Boege, S.J.; Koffas, T.; Kotseroglou, T.; Melissinos, A.C.; Meyerhofer, D.D.; Reis, D.A.; Ragg, W.; Bula, C.; McDonald, K.T.; et al. Studies of nonlinear QED in collisions of 46.6 GeV electrons with intense laser pulses. *Phys. Rev. D* **1999**, *60*, 092004. [CrossRef]
58. Tajima, T.; Mourou, G. Superstrong Fields in Plasmas. In *Superstrong Field in Plasmas, AIP Conference Proceedings*; Lontano, M., Mourou, G., Svelto, O., Tajima, T., Eds.; American Institute of Physics: New York, NY, USA, 2002; Volume 611, pp. 423–436.
59. Dattoli, G.; Gallardo, J.C.; Ottaviani, P.L. Free-electron laser intracavity light as a source of hard X-ray production by Compton backscattering. *J. Appl. Phys.* **1994**, *76*, 1399–1404. [CrossRef]
60. Iracane, D.; Bamas, P. A two-frequency wiggler for better control of free-electron laser dynamics. *Nucl. Instrum. Methods Phys. Res. Sect. A* **1991**, *318*, 839–842. [CrossRef]
61. Basu, C.; Choyal, Y.; Mishra, G.; Dutta, A.K. Analysis of two undulator radiation with low energy correction. *Nucl. Instrum. Methods Phys. Res. Sect. A* **1997**, *388*, 273–281. [CrossRef]
62. Mikhailin, V.; Zhukovsky, K. Two-frequency undulator and harmonic generation of an ultrarelativistic electron. In *Particle Physics at the Year of 250th Anniversary of Moscow University*; Moscow State University: Moscow, Russia, 2006; pp. 393–397. [CrossRef]
63. Drebot, I.; Petrillo, V.; Serafini, L. Two-colour X-gamma ray inverse Compton back-scattering source. *Europhys. Lett.* **2017**, *120*, 14002. [CrossRef]
64. Yoshitaka, T.; Masahiro, K. Gamma-ray vortices emitted from nonlinear inverse Thomson scattering of a two-wavelength laser beam. *Phys. Rev. A* **2018**, *98*, 052130.
65. Zhukovsky, K.V. Generation of UR Harmonics in Undulators with Multiperiodic Fields. *Russ. Phys. J.* **2019**, *62*, 1043–1053. [CrossRef]
66. Zhukovsky, K.V. Analysis of harmonic generation in planar and elliptic bi-harmonic undulators and FELs. *Results Phys.* **2019**, *13*, 102248. [CrossRef]